Conversion of calcium sulphide to calcium carbonate during the process of recovery of elemental sulphur from gypsum waste

M. de Beer[a,b*], J.P. Maree[c], L. Liebenberg[b], and F.J. Doucet[d*]

[a] DST/CSIR National Centre for Nanostructured Materials, Council for Scientific and Industrial Research, PO Box 395, Pretoria 0001, Republic of South Africa.
[b] Centre for Research and Continued Engineering Development, North-West University, Pretoria, Republic of South Africa
[c] Department of Environmental, Water and Earth Science, Faculty of Science, Tshwane University of Technology, Private Bag X680, Pretoria 0001, Republic of South Africa
[d] Industrial Mineralogy Laboratory, Council for Geoscience, Private Bag X112, Pretoria 0001, Republic of South Africa.

* Corresponding authors: mdebeer@csir.co.za (M. de Beer; Tel: +27 (0) 841 4987); fdoucet@geoscience.org.za (F.J. Doucet; Tel: +27 (0) 841 1300)

Abstract

The production of elemental sulphur and calcium carbonate ($CaCO_3$) from gypsum waste can be achieved by thermally reducing the waste into calcium sulphide (CaS), which is then subjected to a direct aqueous carbonation step for the generation of hydrogen sulphide (H_2S) and $CaCO_3$. H_2S can subsequently be converted to elemental sulphur via the commercially available chemical catalytic Claus process. This study investigated the carbonation of CaS by examining both the solution chemistry of the process and the properties of the formed carbonated product. CaS was successfully converted into $CaCO_3$; however, the reaction yielded low-grade carbonate products (*i.e.* < 90 mass % as $CaCO_3$) which comprised a mixture of two $CaCO_3$ polymorphs (calcite and vaterite), as well as trace minerals originating from the starting material. These products could replace the Sappi Enstra $CaCO_3$ (69 mass % $CaCO_3$), a by-product from the paper industry which is used in many full-scale AMD neutralisation plants but is becoming insufficient. The insight gained is now also being used to develop and optimize an indirect aqueous CaS carbonation process for the production of high-grade $CaCO_3$ (*i.e.* > 99 mass % as $CaCO_3$) or precipitated calcium carbonate (PCC).

Keywords

Gypsum waste; carbonation; valorisation; calcium carbonate; calcium sulphide

1. Introduction

The chemical manufacturing industry and the industrial waste remediation sector generate millions of tons of gypsum-rich solid wastes and sludge. Those include processes such as phosphoric, hydrofluoric, citric and boric acid production, treatment of waste from desulphurisation of flue gases from coal-fired power stations, ore smelting, and acid mine water treatment. Most of this poor-quality gypsum is generally regarded as unsuitable for further use, and is therefore stored in large stockpiles. The remediation of acid mine drainage (AMD) using alkaline-based processes gives rise to a gypsum-rich sludge which requires proper environmental management [1] in order to prevent serious environmental pollution such as airborne dust and contamination of groundwater resources. An alternative approach to the often expensive management of stockpiles is to treat the sludge with the aim of converting it into potentially useful products [2].

Gypsum waste can represent a good resource for the recovery of sulphur (S) and calcium carbonate ($CaCO_3$) [3]. Elemental sulphur is an essential raw material for many manufacturing industries such as fertilisers, acids, steel, petroleum, insecticides, titanium dioxide, and explosives [4]. Its application as an alternative feedstock for the production of polymeric materials has also been recently suggested [5]. $CaCO_3$ also has many uses in a wide variety of industrial and commercial applications, either as ground calcium carbonate (GCC; for instance in the manufacturing of concrete or Portland cement, for producing lime to be used in soil stabilization and acid neutralization, for water treatment, and flue gas desulphurization [6]) or as precipitated calcium carbonate (PCC; for instance as a filler and coating pigment in paper, plastics, paints, rubbers and adhesives [7,8].

A multi-step process for the recovery of sulphur and $CaCO_3$ from gypsum waste has been proposed [3]. It involves the following three steps:

(i) Thermal reduction (900°C-1100°C) of gypsum waste to produce calcium sulphide (CaS) using reducing agents (*e.g.* solid carbon materials such as coal or activated carbon (Eq. (1); [9,10]), carbon monoxide gas (Eq. (2); [11,12]), or hydrogen gas (Eq. (1); [13])).

$$CaSO_4\,(s) + 2C\,(s) \rightarrow CaS\,(s) + 2CO_2\,(g) \quad (1)$$
$$CaSO_4\,(s) + 4CO\,(g) \rightarrow CaS\,(s) + 4CO_2\,(g) \quad (2)$$
$$CaSO_4\,(s) + 4H_2\,(g) \rightarrow CaS\,(s) + 4H_2O\,(\ell) \quad (3)$$

(ii) Direct aqueous carbonation of CaS to produce hydrogen sulphide (H_2S) and $CaCO_3$. The reaction proceeds according to Eq. (4).

$$CaS\,(s) + H_2O + CO_2\,(g) \rightarrow H_2S\,(g) + CaCO_3\,(s) \quad (4)$$

(iii) Recovery of elemental sulphur from H_2S via the commercially available chemical catalytic Claus process [14].

Two steps of the process (steps (i) and (iii)) are fairly well understood [15,16], but little effort has been given to the investigation of the second step, except for two independent studies on the stripping of H_2S [3], and on the conversion of CaS into H_2S and $CaCO_3$ but making use of methyldiethanolamine (MDEA) as a CO_2 and H_2S solubility catalyst [17]. The primary objective of this paper, which focuses on step (ii) above (eq. (4)), was therefore to provide a better understanding of the direct aqueous carbonation reaction between CaS and CO_2, by investigating both the solution chemistry of the process and the properties of the formed carbonated product.

2. Experimental section

2.1 Materials preparation and characterization

A calcium sulphide-rich calcine powder (hereafter denominated CaS_r) was produced from a gypsum waste sample collected at an acid mine water neutralisation plant in South Africa. CaS_r was generated in an electrically heated kiln at 1080°C using an existing thermal reduction process with

duff coal as the reducing agent [15]. The sample was then stored in sealed plastic bags inside a container filled with nitrogen gas to ensure its stability and to avoid spontaneous oxidation to $CaSO_4$ [18].

The elemental and mineralogical compositions of the gypsum waste sample, CaS_r and the formed carbonate products were analysed using XRF (PANanalytical Axios X-ray fluorescence spectrometer equipped with a 4 kW Rh tube) and XRD (Bruker D8 Advance X-ray diffractometer), respectively. The samples were micronized to sub-30 µm particle size for increased accuracy prior to XRD analysis. The samples were further characterised for their total carbon and sulphur content using an Eltra CS800 Carbon & Sulphur analyser (Eltra GmbH, Germany).

2.2 Direct aqueous carbonation experiments

Industrial-grade carbon dioxide (CO_2; Air Liquide, South Africa) was used in all carbonation experiments. The rationale for using CO_2 in a direct carbonation setup was that i) it promotes CaS dissolution in water, ii) it induces the stripping of hydrogen sulphide gas (H_2S) from solution, and iii) it stimulates the carbonation of solubilized calcium derived from CaS dissolution to form calcium carbonate.

All experiments were performed in a 3-liter Perspex stirrer tank batch reactor equipped with four equally spaced baffles. The reactor was equipped with a sparger with small diameter (< 1mm) openings for the introduction of the CO_2 gas. A mechanical overhead stirrer (RW 20 digital from IKA®-Werke GmbH & Co. KG, Germany) and a Rushton impeller (manufactured by Manten Engineering, South Africa) were used for mixing. The Rushton impeller had six vertical blades which are fixed onto a disk. This disk design ensured that most of the torque of the motor was consumed at the tips of the agitator. The CO_2 gas flow rate was controlled using a rotameter (Fisher & Porter, model 10A6132M/T62). All experiments were conducted at atmospheric pressure (Pretoria, South Africa).

CaS_r was subjected to direct aqueous carbonation and stripping in a one-step process. A preliminary experiment was performed under set conditions to better understand the prevailing processes. For this purpose, CaS_r was first dispersed in distilled water to obtain a 10 wt% CaS_r slurry. After 30 min of continuous mixing at 300 min^{-1}, CO_2 gas was introduced at a constant flow rate of 2.94 ℓ CO_2/min/kg CaS_r into the slurry. The pH, electrical conductivity and temperature of the suspension were logged using a Hanna HI 2829 multiparameter logger at 5 second intervals to collect time-series data on the dynamics of the system. The reaction was terminated when the pH and electrical conductivity remained unchanged for 10 to 15 min.

Upon completion, the suspension was removed from the reactor and filtered using Whatman grade no. 1 filter paper; the filter cake was thoroughly rinsed with water, dried at mild temperature (*i.e* 60° C; to prevent thermal conversion of gypsum [19]) for 24 h and characterized by XRD and high-vacuum SEM. Throughout the experiments, sub-samples of the suspensions were collected from the reactor at regular intervals and filtered using 0.45µm PALL acrodisc PSF GxF/GHP membranes (Microsep (Pty) Ltd, South Africa). The filtrates were analysed for their calcium and sulphide content. Total sulphide concentration (sum of dissolved H_2S, HS^- and S^{2-}) of the filtrates was determined iodometrically, where an excess of added iodine was titrated back with sodium

thiosulfate. The analysis was carried out manually on filtered (for soluble sulphide) and unfiltered (for total sulphide, *i.e.* in both solution and solid phases) samples according to procedures 4500-S^{2-}/Iodometric method described in Standard Methods [20]. The sulphide in the solid phase and the sulphide stripped from solution were calculated by difference. The concentration of calcium ions in solution was determined by direct complexometric titration with ethylene-diamine tetraacetate (EDTA) according to the procedure 3500-Ca/EDTA titrimetric method [20]. High-vacuum scanning electron micrographs were collected using a JEOL JSM7500 microscope to obtain information on morphologies and size distribution of the solid materials. Samples were dispersed on carbon tape and sputter-coated with a thin, conductive layer of gold using a Emitech K950X sputter coater. The acceleration voltage was 2 kV.

The preliminary experiment was followed by a second set of experiments, where the effect of the stirring rate (180 *vs* 300 *vs* 480 min^{-1}) on solution dynamics and the influence of the CO_2 flow rate (2.53 *vs* 8.80 *vs* 14.83 *vs* 29.33 *vs* 44.00 ℓ CO_2/min./kg calcine) on both solution dynamics and the $CaCO_3$ particle characteristics were also studied.

3. Results and Discussion

3.1 Materials characterization

The XRD pattern of the untreated gypsum waste demonstrated that the primary mineral phase was gypsum ($CaSO_4.2H_2O$; 96.9%), which co-existed with magnesite ($MgCO_3$; 3.1%). The amount of gypsum contained in the waste was further confirmed by the total content of calcium and sulphur determined by XRF (Table 1) and by carbon and sulphur analysis (Table 2) respectively. The sample

Table 1 Chemical composition (wt %) of starting material and formed products.

	SiO_2	Al_2O_3	$Fe_2O_{3(t)}$	MgO	CaO	SO_3	LOI[1]
Untreated gypsum	0.13	0.08	0.03	0.27	30.18	47.71	21.59
wasteCaS_r	4.07	2.58	0.90	0.07	50.84	60.41	-21.60[2]
Formed carbonate	3.21	2.14	1.17	0.02	40.01	5.92	44.73

[1] Loss on ignition

[2] Sample CaS_r exhibited a negative loss on ignition. This characteristic suggested the possible occurrence of a weight increase arising from the oxidation of CaS to $CaSO_4$, which would have been higher than the weight loss caused by removing volatiles from the mineral structures. Similar observations were already made for iron-rich coal ashes, in which case negative loss on ignition was best explained by the oxidation of Fe^{2+} to Fe^{3+} (FeO to Fe_2O_3) and its associated weight increase [35].

Table 2 Carbon and sulphur content (wt %) of starting material and formed products.

	C	S
Untreated gypsum waste	0.29	18.17
CaS_r	16.76	28.65
Formed carbonate	20.91	3.37

was characterised by a mean diameter D(v,0.5) of 43.86 µm, with 90% of the particles being smaller than 176.70 µm. The gypsum waste was converted into CaS_r by thermal reduction in an electrically heated kiln at 1080°C, using duff coal as the reducing agent [15].

The bulk mineralogical composition of CaS_r was also determined. The most abundant mineral was calcium sulphide (CaS; 50.7%), also called oldhamite. Less abundant mineral phases included hydroxyapatite ($Ca_{8.86}(PO_4)_6(H_2O)_2$), quartz ($SiO_2$), anhydrite ($CaSO_4$), and lime (CaO). The sample contained 50.84% Ca (Table 1) and 28.65% elemental sulphur (Table 2), which were present as both calcium sulphide and anhydrite (for Ca and S), as well as hydroxyapatite (for Ca). CaS_r contained some impurities (*e.g.* Al, Fe; Table 1), which originated most probably from duff coal used during the thermal reduction process.

3.2 Solution chemistry

Theoretically, the direct reaction between solid CaS dispersed in water and CO_2 produces H_2S gas and precipitated $CaCO_3$ according to Eq. (5). The reaction involves at least four primary coexistent mechanisms: (i) aqueous dissolution of CaS and other soluble mineral phases, (ii) aqueous dissolution of CO_2, (iii) precipitation of carbonates, and (iv) stripping of H_2S.

$$CaS\ (s) + H_2O\ (ℓ) + CO_2\ (g) \rightarrow H_2S\ (g) + CaCO_3\ (s) \qquad (5)$$

The dynamics existing and evolving between these four mechanisms in the CaS-H_2O-CO_2-H_2S system was investigated by monitoring the profile of several solution parameters over time: conductivity and temperature (Figures 1a and 1b respectively), and pH and the chemical distribution of sulphide species between solid, liquid and gaseous phases (Figure 2).

Preliminary experiment – Solid CaS_r was initially suspended in water (no CO_2) and was continuously mixed for 30 min. Solution pH increased rapidly from 6.35 to 11.56 within the first minute, and stabilized at 11.71 after about 2 minutes of stirring. This was accompanied by an increase in solution conductivity (*ca.* 2.5 mS/cm) and temperature (ΔT 0.16°C), and in the concentration of soluble sulphur (9 mmol/l as S) and calcium (9 mmol/l as Ca); these observations could be ascribed to the dissolution of CaS present in CaS_r. The dissolution of anhydrite and hydroxyapatite cannot be discounted and may have contributed to the release of some calcium (Ca^{2+}) and sulphur (S^{2-}) in solution, although only to a small extent in comparison to CaS. CaS dissolution proceeded via the

A.

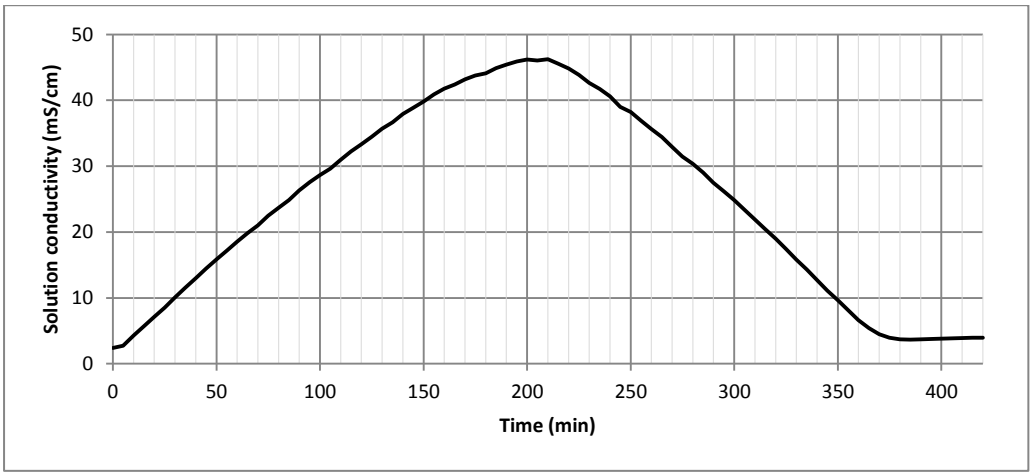

B.

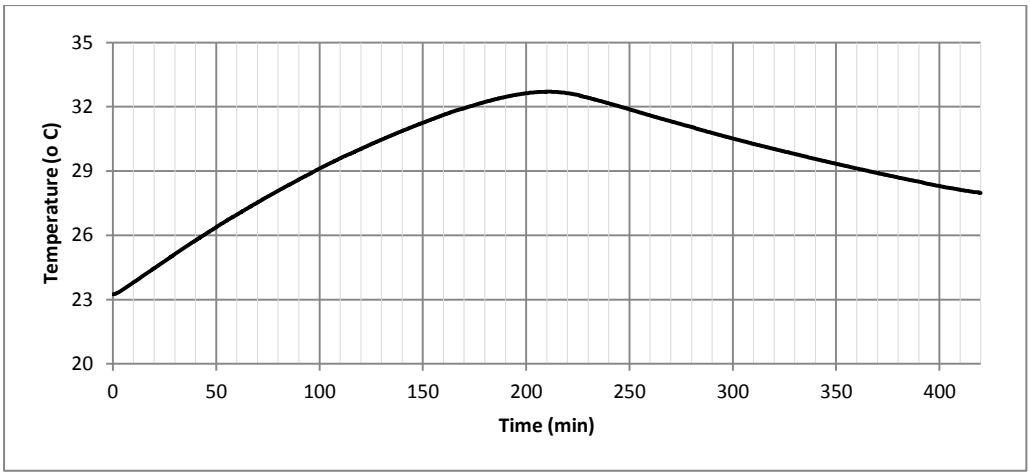

Figure 1 Solution conductivity (a) and temperature (b) profiles for the direct aqueous carbonation of the calcine sample suspended in distilled water (CaS slurry containing 22.7g calcine/ℓ; initial pH: 11.7; gas flow: 2.94 ℓ CO_2/min/kg calcine; mixing rate: 180 min^{-1}).

release of Ca^{2+} and S^{2-} ions in water, with S^{2-} subsequently binding with proton ions from the water molecules and thereby generating equimolar amounts of hydroxide ions (OH^-). As a result, a solution containing soluble calcium hydrosulfide ($Ca(HS)_2$) (Eq. (6); [21]), which was characterized by a pH of 11.71 (Figure 2), was generated. CaS is a sparingly soluble salt in water and reported values for its solubility at 25°C varies widely, with published values ranging from 0.125 g/l to 1.0 g/l [22-24]. The difference can be ascribed to the complicated dissolution mechanisms involved. The high sulphur content (733 mmol/l as S) of the solids dispersed in water and the low amount (9 mmol/l as S) of dissolved S in solution measured following a period of 30 min of dissolution prior to the addition of CO_2 (time = 0 min) confirmed the low solubility of CaS in water (Figure 2).

$$2CaS\ (s) + 2H_2O\ (\ell) \leftrightarrow Ca(HS)_2\ (aq) + Ca(OH)_2\ (s) \qquad (6)$$

Following the addition of CO_2 to the aqueous CaS suspension, temporal changes in the conductivity and temperature of the solution were observed. They exhibited similarly-shaped profiles, with both

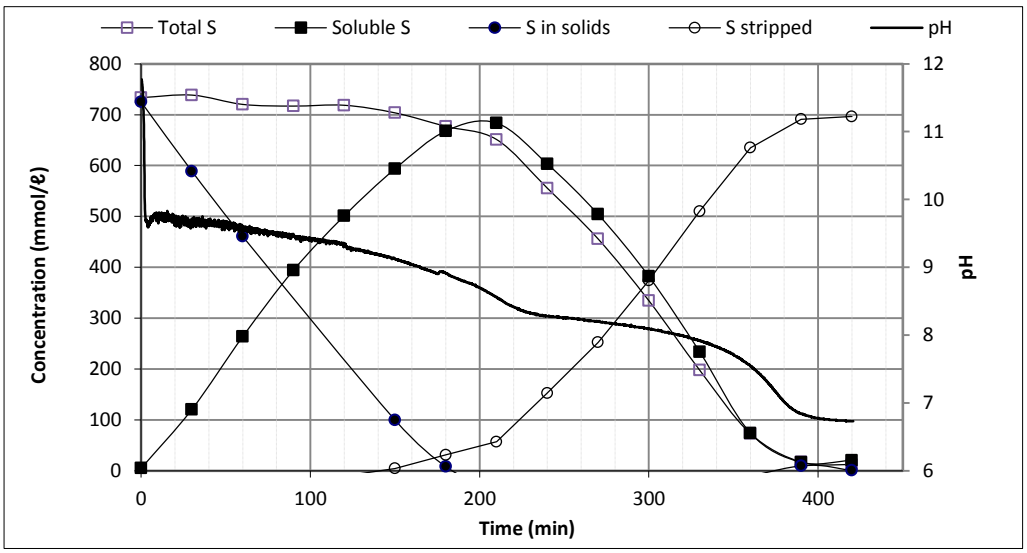

Figure 2 Changes in the chemical distribution of sulphide species between solid, liquid and gaseous phases during direct aqueous carbonation of the calcine sample (CaS slurry containing 22.7g calcine/ℓ; initial pH: 11.7; gas flow: 2.94 ℓ CO_2/min/kg calcine; mixing rate: 180 min^{-1}; 'total S' refers to total sulphur contained in the reactor, *i.e.* soluble sulphur + sulphur in solids).

parameters having reached their maxima after 200-210 min of reaction (Figure 1). These profiles correlated closely with the one found for the distribution of soluble sulphur species (Figure 2). When adding CO_2 (time = 0 min), the pH initially dropped sharply from 11.7 to 9.6 within a short period of time (< 1 min), after which it continued decreasing more gradually down to *ca.* 6.8. The gradual drop in pH exhibited 3 different slopes: (1) from 1 to 125 min, (2) from 125 to 210 min, and (3) from 210 to 240 min, before stabilizing at about 6.8 from 250 min onwards.

During the first stage of the reaction (0 to 200 min), the total S concentration in the reactor remained constant at about 708 mmol/l (as S). The S concentration in solution increased steadily to a maximum of 684 mmol/l whilst the S content in the undissolved material decreased at the same rate from about 730 mmol/l to about 8 mmol/l. The steady increase in dissolved S upon CO_2 addition, which was not observed in the absence of CO_2, indicated the greater solubility of CaS in water in the presence of dissolved CO_2. This was further confirmed by the increase in solution conductivity from 2.57 to 43.8 mS/cm during the first 120 min. During this time, little, if any, S was stripped from the system (as indicated by the constant total S concentration in the reactor), which can be explained by the hydrogen sulphide speciation diagram (Figure 3) illustrating the required pH conditions for H_2S formation. The diagram was obtained by calculating the fractional composition of the sulphide species in water using the dissociation constants for hydrogen sulphides at 25°C. The ionization of H_2S in water proceeds in two steps and can be calculated from the dissociation constants ($K_1 = 9.1 \times 10^{-8}$ and $K_2 = 1.1 \times 10^{-12}$; [23]) and Eq. 7 and 8.

$$H_2S\ (aq) + H_2O\ (l) \leftrightarrow HS^-(aq) + H_3O^+\ (aq);\quad pKa_1 = 7.04 \qquad (7)$$

$$HS^-\ (aq) + H_2O\ (l) \leftrightarrow S^{2-}(aq) + H_3O^+\ (aq);\quad pKa_1 = 11.96 \qquad (8)$$

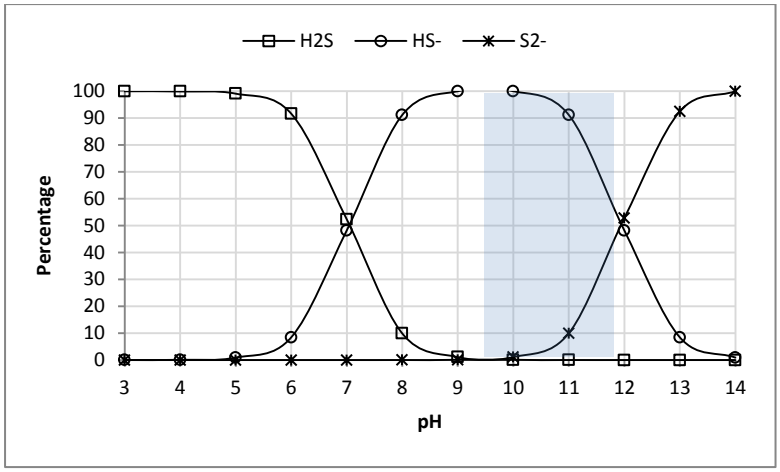

Figure 3 The hydrogen sulphide speciation diagram.

Temporal chemical analysis of the soluble sulphide and soluble calcium species (Figure 4, time = 0 to 120 min) showed that one mole of $Ca(HS)_2$ was formed for every two moles of CaS dissolved in the reactor, which is in agreement with Eq. (9).

$$2CaS\ (s) + CO_2\ (g) + H_2O\ (aq) \leftrightarrow Ca(HS)_2\ (aq) + CaCO_3\ (s) \qquad (9)$$

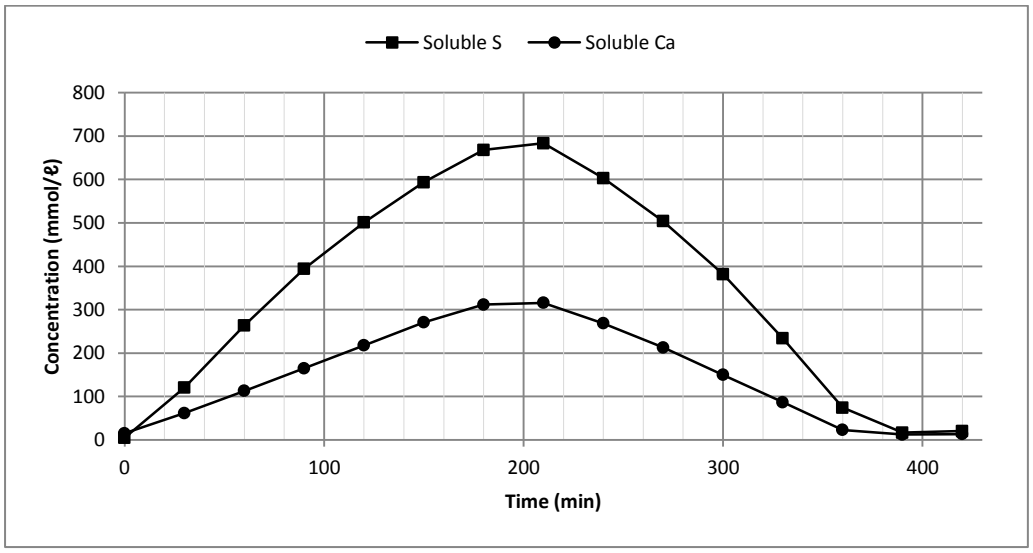

Figure 4 The distribution of soluble sulphide and soluble calcium concentrations with time of a calcine slurry in equilibrium with distilled water upon CO_2 addition (CaS slurry containing 22.7 g/l as S; initial pH: 11.7; gas flow: 2.94 l CO_2/min./kg calcine; stirring rate: 180 min^{-1}).

3.3 Effect of stirring rate

Solution dynamics – Figure 5 shows the effect of the stirring rate on CaS dissolution and H_2S stripping from the calcine slurry. During the first stage of the reaction, the electrical conductivity increased mainly as a result of CO_2 gas absorption and CaS dissolution, and decreased in the second stage as a

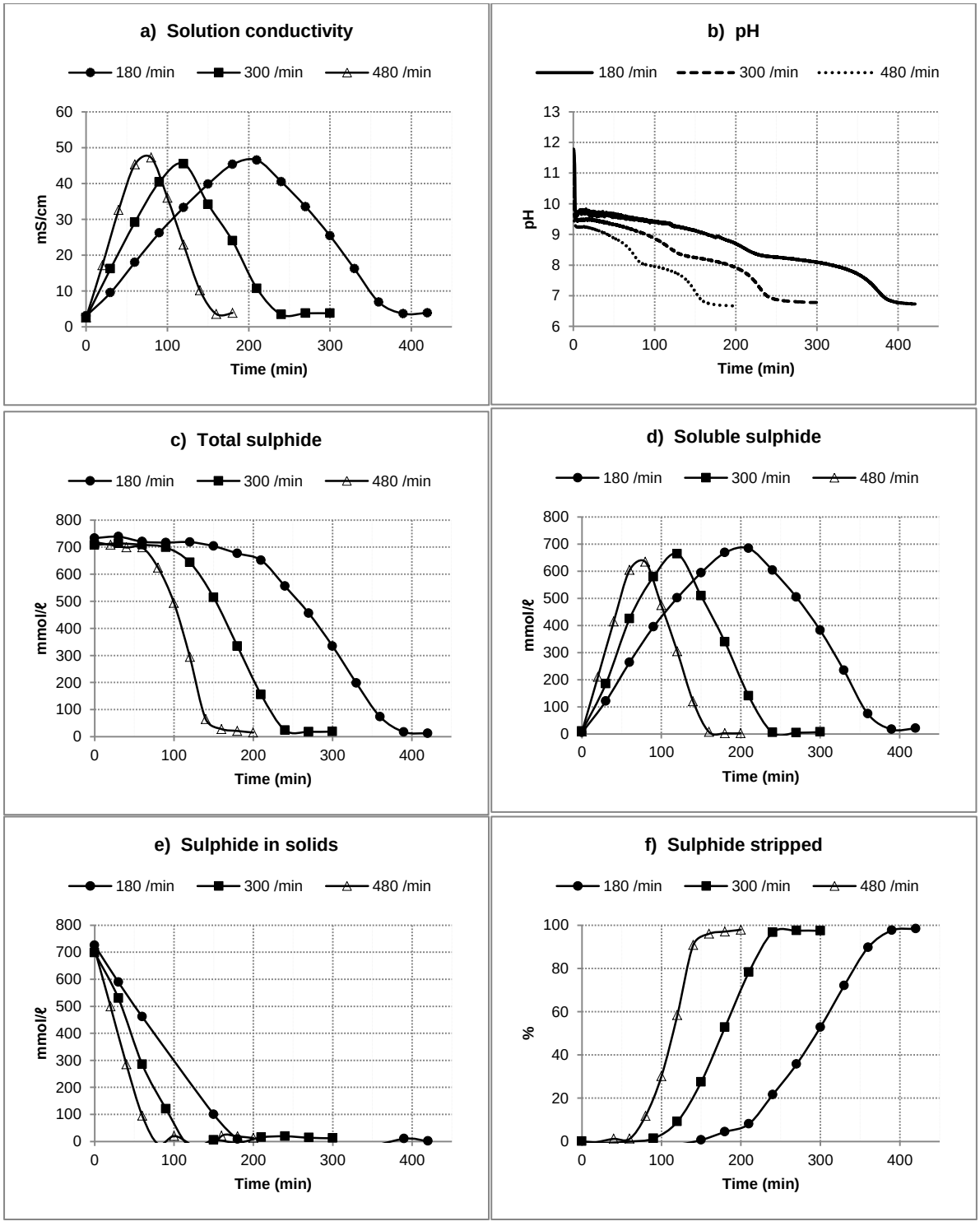

Figure 5 Effect of stirring rate on a) the solution conductivity, b) pH, c) total sulphide concentration, d) soluble sulphide concentration, e) sulphide in solid phase and f) sulphide stripped from solution with time (CaS slurry containing 22.7 g /ℓ as S; initial pH: 11.7; gas flow-rate: 2.94 ℓ CO_2/min/kg calcine).

result of H_2S gas stripping and $CaCO_3$ precipitation (Figure 5 (a)). With a stirring rate of 180 min^{-1} the reaction was complete (as indicated by levelling off of all the salient parameters) in approximately 390 min, while the use of a stirring rate of 300 min^{-1} and 480 min^{-1} reduced the completion time of

the reaction down to approximately 240 min and 160 min, respectively. Both the rate of CaS dissolution and H_2S were positively influenced by faster stirring rates (Figure 5 (a)-(f)). The Rushton impeller used in this study was a radial flow type specially designed to provide high shear conditions required for breaking gas bubbles and thereby increasing the rate of gas transfer. In systems where mass transport is the rate-determining step, it is possible to increase the reaction rate by increasing the mass transfer rate [25]. For solid particles, the interfacial area is generally determined by the physical appearance of the particle and there is therefore little benefit in increasing the stirring rate. However, for gas reactions an increase in stirring rate can generate smaller bubbles and can consequently increase the interfacial area of CO_2 gas bubbles. The increased interfacial area of the gas phase is directly related to an increase in the mass transfer rate [26]. The current experiments confirmed that faster reaction rates could be achieved by increasing stirring rates in the case of direct aqueous carbonation reactions. Table 4 illustrates that an increase in the stirring rate accelerated both the CaS dissolution reaction as well as the carbonation reaction.

3.4 Effect of CO_2 flow rate

Solution dynamics – The effect of the CO_2 gas flow rate on the temporal distribution of soluble sulphide concentrations was investigated. A summary of the calculated reaction rates for various CO_2 flow rates is presented in Table 5. As shown in Figure 6, the reaction was complete (as indicated

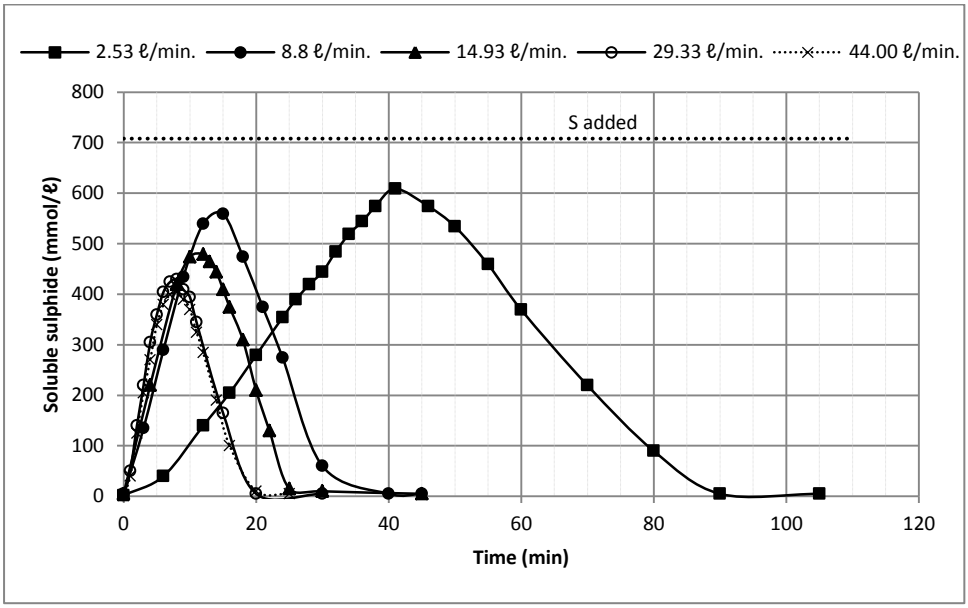

Figure 6 The effect of gas flow-rate (ℓ CO_2/min/kg calcine) on the distribution of the soluble sulphide concentration with time (CaS slurry containing 22.7 g/ℓ as S; initial pH: 11.7; stirring rate: 600 min^{-1}).

by the levelling off of soluble sulphide concentration) in approximately 86 min at a flow-rate of 2.53 ℓ CO_2/min/kg CaS_r, while at 8.80, 14.93 and 29.33 ℓ CO_2/min/kg CaS_r, the reactions were completed in 38, 26 and 18 min, respectively. The dissolution of gaseous CO_2 in solution is generally the first rate-limiting step in direct carbonation reactions [27], but it can be enhanced by increasing the CO_2 flow rate [28] when working at atmospheric pressure and thereby ensuring that excess carbonate ions are present relative to calcium ions. However, a further increase of the flow rate to more than 29.33 ℓ CO_2/min/kg CaS_r had little effect on the overall reaction time (Table 5 and Figure 6). If the

solubilisation of CO_2 was the limiting factor, no further improvement in CO_2 dissolution with increased flow rates would be evident due to the solubility of CO_2, which is constant at the given conditions. For example, at 25°C and 1 atmosphere, the solubility of CO_2 is about 0.09 ℓ CO_2 per 100 ml of water [29]. When the CO_2 gas flow rate is higher than the solubility of CO_2 gas in water, the excess CO_2 gas cannot be adsorbed and will run through the system, eventually escaping from solution in the gas phase. Under the specific experimental conditions, it is also possible that the dissolution of CaS might have been the rate-limiting step (not further investigated to confirm this mechanism). If solubilisation of calcium was slower than CO_2 dissolution, the overall reaction time will also not increase upon increased CO_2 flow rates.

It was also observed that the maximum sulphide concentration measured in solution was lower than that of total sulphide added to the system as CaS (*i.e.* 708 mmol/ℓ as S) for all CO_2 flow rates tested (Figure 6). Given that the sulphur content of all the carbonate products generated at different CO_2 flow rates was very low (< 0.15 mass % (as S)), the loss of sulphur from the system could essentially be attributed to the escape of volatile H_2S gas.

$CaCO_3$ produced – The effect of CO_2 flow rate on the crystal structure and polymorphism of the formed $CaCO_3$ products was also investigated. $CaCO_3$ has three anhydrous crystalline forms (*i.e.* calcite, aragonite and vaterite). In this study, calcite and vaterite were the only polymorphs of $CaCO_3$ that were identified, regardless of the CO_2 flow rate used (Tables 3 and 6). The distribution of the

Table 3 Mineralogical composition (wt %) of low-grade calcium carbonate formed, as determined by XRD using Rietveld refinement.

Mineral	Chemical formula	Low-grade $CaCO_3$[1] (wt %)
Calcite	$CaCO_3$	87.65
Vaterite	$CaCO_3$	0.59
Fluorite	CaF_2	1.22
Quartz	SiO_2	1.62
Apatite	$Ca_5(PO_4)_3OH$	3.46
Anhydrite	$CaSO_4$	5.40
Oldhamite	CaS	0.05

[1] Low-grade $CaCO_3$ is a published terminology [6] which refers to carbonate material containing < 90 mass % as $CaCO_3$.

Table 4 Effect of stirring rate on reaction rate (CaS slurring containing 22.7g S/ℓ; initial pH: 11.7; gas flow-rate: 2.94 ℓ CO_2/min/kg calcine).

Stirring rate (min^{-1})	Process step	Rate (g/ℓ/min (as S))	Standard deviation (±)	R^2
180	CaS dissolution	0.116	0.002	0.9975
	H_2S stripping	-0.127	0.002	0.9972
300	CaS dissolution	0.218	0.005	0.9954
	H_2S stripping	-0.205	0.002	0.9993
480	CaS dissolution	0.355	0.013	0.9948
	H_2S stripping	-0.313	0.005	0.9985

combined $CaCO_3$ phases reached 86-88 mass % (the sum of calcite and vaterite) in every sample produced, whilst mineral impurities (sum of all the non-$CaCO_3$ mineral phases) amounted to 12-14 mass %. $CaCO_3$ discoloring could not be satisfactorily explained by the presence of the mineral impurities detected by XRD (Tables 3 and 6); it was probably due to ash from the duff coal used as reducing agent in the thermal reduction step, and possibly to a lesser extent to iron impurities (1.17% $Fe_2O_{3(t)}$; Table 1). Based on their carbonate contents, the greyish products (Figure S1)

Supplementary Figure S1 Representative photograph of the low-grade $CaCO_3$ product formed via the direct aqueous CaS process.

obtained were classified as low-grade $CaCO_3$ (< 90 mass % as $CaCO_3$; [6]). The XRD results showed that at the lowest CO_2 flow rate of 2.5 ℓ CO_2/min/kg CaS_r, the product was mainly composed of calcite. Samples prepared at higher CO_2 flow rates showed the presence of binary mixtures of calcite and vaterite, with a progressive decrease in mole fraction of calcite and a corresponding increase of vaterite with increased CO_2 flow rates. Figure 7 depicts a clearer view on the variation in the proportion of calcite to vaterite produced at different CO_2 flow rates. Therefore, although the total $CaCO_3$ content of produced low-grade $CaCO_3$ was not significantly different between the CO_2 flow rates tested, the distribution ratio of calcite and vaterite was greatly influenced by the CO_2 flow rate. For all flow rates tested, the conversion of CaS was complete, with only trace amounts (< 0.1%) of CaS detected in the produced materials.

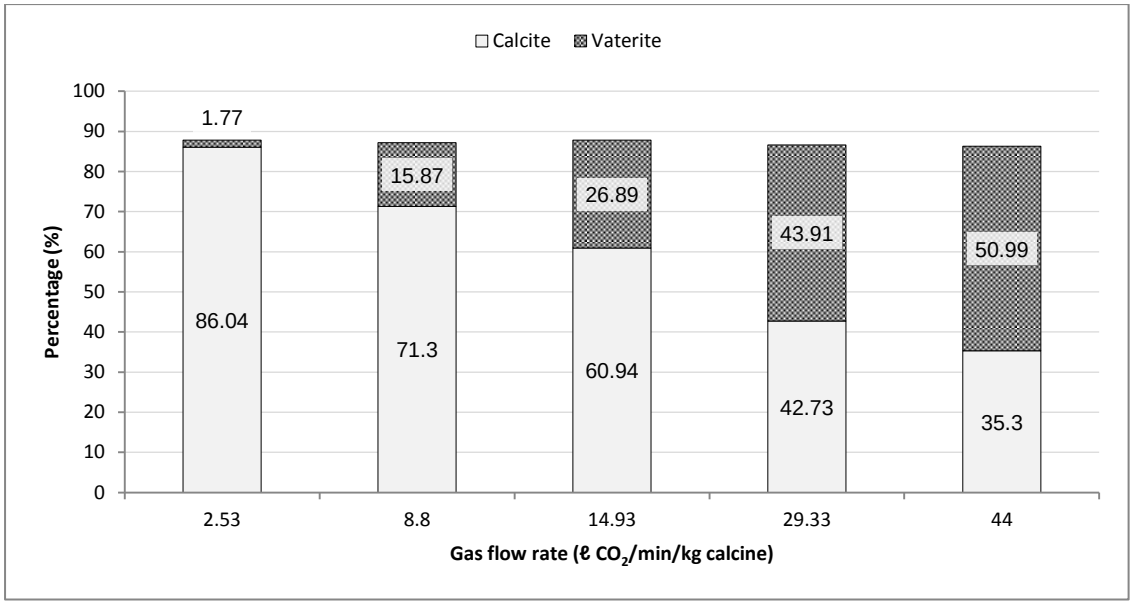

Figure 7 The distribution ratio of calcite and vaterite polymorphs in the low-grade $CaCO_3$ products formed at various CO_2 gas flow rates (CaS slurry containing 22.7 g/ℓ as S; initial pH: 11.7; stirring rate: 600 min^{-1}).

Table 5 Effect of the CO_2 flow rate on reaction rate (CaS slurry containing 22.7g S/ℓ; initial pH: 11.7; stirring rate: 600 min^{-1}).

CO_2 flow (ℓ/min/kg calcine)	Process step	Reaction kinetics			Reaction time (min)	Actual	
		Rate (mmol/ℓ/min (as S))	Standard deviation (±)	R^2		Actual (g/100g CaS_r)	% yield
2.53	CaS dissolution	16.08	0.43	0.9929	86	127.3	91.7%
	H_2S stripping	-13.57	0.57	0.9913			
8.80	CaS dissolution	45.57	1.58	0.9964	38	127.5	91.9%
	H_2S stripping	-21.82	4.36	0.8931			
14.93	CaS dissolution	47.87	3.06	0.9919	26	126.5	91.2%
	H_2S stripping	-30.76	2.93	0.9402			
29.33	CaS dissolution	65.12	4.16	0.9761	18	128.1	92.3%
	H_2S stripping	-38.34	1.92	0.9925			
44.00	CaS dissolution	61.81	3.65	0.9795	18	130.6	94.1%
	H_2S stripping	-36.88	2.27	0.9814			

Table 6 Mineralogical composition of low-grade $CaCO_3$ produced at different CO_2 gas flow rates (CaS slurry containing 22.7 g/ℓ as S; initial pH: 11.7; stirring rate: 600 min^{-1}).

Mineral composition (mass%)*	CO_2 flow-rate (ℓ CO_2/min/kg calcine)				
	2.5	**8.8**	**14.9**	**29.3**	**44.0**
Calcite	86.0	71.3	60.9	42.7	35.3
Anhydrite	4.5	3.4	3.2	3.1	3.6
Vaterite	1.8	15.9	25.9	43.9	51.0
Quartz	1.9	3.0	2.0	2.5	2.5
Apatite	4.1	4.7	5.1	5.7	5.6
Fluorite	1.4	1.2	1.3	1.3	1.1

* Only minerals present in amounts larger than 1% are reported.

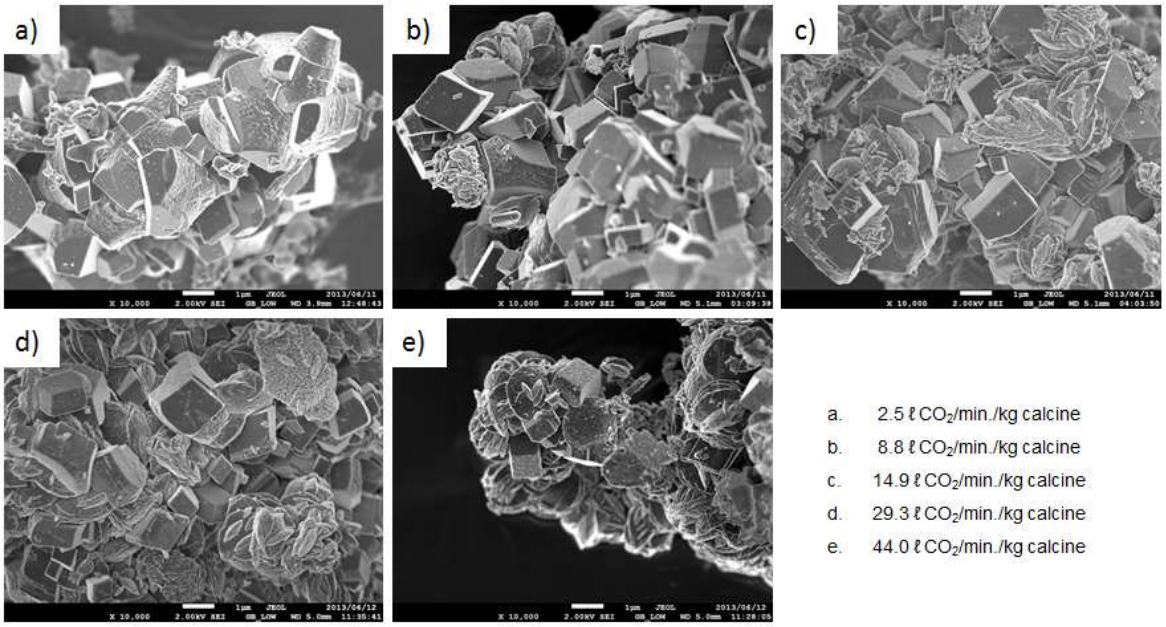

Figure 8 Low-magnification SEM micrographs of low-grade $CaCO_3$ products formed at various CO_2 gas flow rates (CaS slurry containing 22.7 g/ℓ as S; initial pH: 11.7; stirring rate: 600 min^{-1}).

SEM micrographs of the samples produced at different CO_2 flow rates confirmed the distribution between the two polymorphs identified by XRD (Figure 8). The two prevalent $CaCO_3$ phases can clearly be distinguished by their characteristic morphologies. Vaterite can be recognised as the lens-shaped particles [30] whilst calcite was identified as rhombohedral crystallites [31]. All precipitates were micron-sized lumps made up of randomly aggregated rhombohedra of calcite and lens-shaped (or ellipse-like) vaterite. The product generated at 2.5 ℓ CO_2/min/kg CaS_r consisted mostly of irregular polyhedron calcite crystals (Figure 8a). Some crystal planes of the irregular polyhedron structure were flat with smooth surfaces, while other planes were rough with a "step" structure. At higher CO_2 flow rates, mixtures of vaterite and calcite were found (Figures 8b-e). Interpenetrated rhombohedral cubes of calcite with smooth surfaces and mixtures of ragged and sharp edges were

identified. Calcite particles aggregated to form large, irregular particles and were partly overgrown by clusters of vaterite (Figures 8b-e). It was also observed that only lens-shape vaterite particles had been formed in this study, and no classical spherical vaterite particles had been identified. Figure 9a shows a higher magnification of Figure 8c, whilst Figure 9b exhibits a higher magnification of Figure 8e to illustrate the detail of the lens-shape vaterite crystals.

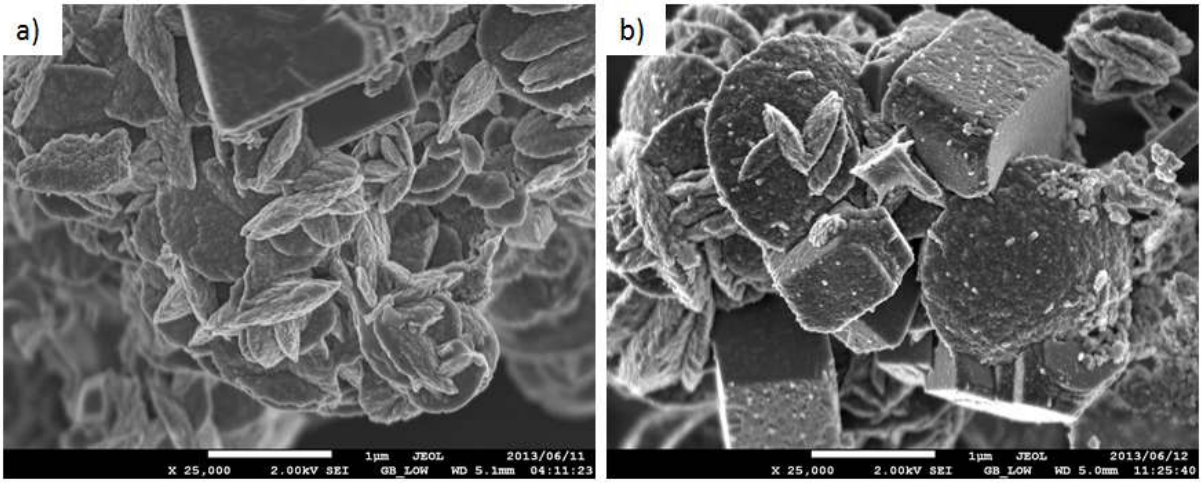

Figure 9 SEM micrographs of low-grade $CaCO_3$ products at 25 000 × magnification showing the lens-shaped crystals of vaterite produced at a) 14.5 and b) 44.0 ℓ CO_2/min/kg calcine respectively (CaS slurry containing 22.7 g/ℓ as S; initial pH: 11.7; stirring rate: 600 min^{-1}).

The median size D(v,0.5) of the particles produced at CO_2 flow rates between 2.53 and 44.00 ℓ/min/kg calcine varied between 16.1 and 21.3 µm. No significant reduction in median particle sizes was observed when using higher CO_2 flow rates, which was in agreement with published findings [32]. Approximately 0.95 kg low-grade $CaCO_3$ (< 90 mass% as $CaCO_3$) was produced for every 1 kg of CaS_r processed. Actual yields were independent of the CO_2 flow rate.

3.5 Estimated economic feasibility

On the basis of our laboratory studies, the recovery of $CaCO_3$ and sulphur (S recovery studies not included in this paper) from gypsum waste is economically promising. The treatment of 1 ton of waste gypsum yields 0.58 ton of $CaCO_3$ (valued at R145) and 0.19 ton of sulphur (valued at R294). The price of $CaCO_3$ and sulphur were taken as R250/t and R1550/t respectively (average values from 2007 to 2011, for limestone sales in South Africa and S imports to South Africa [33]). This compares favourably with the input cost of the main raw material, coal. 0.14 ton of coal is needed for the thermal reduction of 1 ton of waste gypsum to CaS. At a coal cost of R400/t, the input cost of the coal amounts to R56/t waste gypsum. This is significantly less than the combined value of the products, R383 for $CaCO_3$ and sulphur (the energy requirement of the thermal process was not taken into account). The major advantage of the process of conversion of gypsum waste to commercial-grade products lies in the savings on gypsum waste disposal costs. Long-term storage and management of gypsum waste dumps present economic as well as potential environmental challenges. Not only are these dumps unsightly, but they also occupy large areas of land and require long-term expenditures for maintenance and monitoring.

4. Conclusions

The production of elemental sulphur and $CaCO_3$ from gypsum waste can be successfully achieved by combining the thermal reduction of gypsum into calcium sulphide (CaS), followed by the direct aqueous carbonation of CaS for the generation of hydrogen sulphide (H_2S) and $CaCO_3$, and the subsequent conversion of H_2S into S via the commercially available chemical catalytic Clauss process. While the overall process can successfully produce elemental sulphur, this study has shown that direct carbonation can only yield low-grade $CaCO_3$ products (*i.e.* < 90 mass % as $CaCO_3$), which are made up of binary mixtures of calcite and vaterite, with a progressive decrease in mole fraction of calcite and corresponding increase of vaterite with increased CO_2 flow rates. These formed materials could replace the Sappi Enstra $CaCO_3$ (69 mass % $CaCO_3$), a by-product from the paper industry which is used in many full-scale AMD neutralisation plants in South Africa [34] but is becoming insufficient. The insight gained on the solution chemistry and the characteristics of formed $CaCO_3$ derived from this study on the direct aqueous CaS carbonation process has also served as the basis for our current effort in developing and optimising indirect aqueous CaS carbonation processes for the production of high-grade $CaCO_3$ (*i.e.* > 99 mass % as $CaCO_3$) or precipitated calcium carbonate (PCC).

Acknowledgments

The authors thank the following organisations for financial support and/or technical/scientific input: THRIP (Technology and Human Resource for Industry Programme of the National Research Foundation (NRF)), Tshwane University of Technology (TUT), North-West University (NWU), the Council for Scientific and Industrial Research (CSIR) and the Council for Geoscience (CGS).

References

[1] F. Macías, M.A. Caraballo, J.M. Nieto, Environmental assessment and management of metal-rich wastes generated in acid mine drainage passive remediation systems, J. Hazard. Mater. 229-230 (2012) 107-114.

[2] D. Tao, S. Chen, B.K. Parekh, M.T. Hepworth, An investigation of a thermochemical process for conversion of gypsum and pyrite wastes into useful products, Adv. Environ. Res. 5 (2001) 277-284.

[3] N.R. Nengovhela, C.A. Strydom, J.P. Maree, S. Oosthuizen, D.J. Theron, Recovery of sulphur and calcium carbonate from waste gypsum, Water SA 33 (2007) 741-747.

[4] D.J. Cork, D.E. Jerger, A. Maka, Biocatalytic production of sulphur from process waste streams, Biotechnol. Bioeng. 16 (1986) 149-162.

[5] D.J. Cork, D.E. Jerger, A. Maka, Biocatalytic production of sulphur from process waste streams, Biotechnol. Bioeng. 16 (1986) 149-162.

[6] J.A.H. Oates, Lime and limestone: Chemistry and technology, production and uses. Wiley-VCH Verlag GmbH, Weinheim, 1998.

[7] M. Windholz, The Merck Index, tenth ed., Merck & Co., Inc., New Jersey, 1983.

[8] W. Zhang, X. Li, Z. Qu, Q. Zhao, G. Chen, Facile solution synthesis and characterization of $CaCO_3$ microspheres with urchin-shaped structure, Mater. Lett. 64 (2010) 71-73.

[9] L. Ma, X. Niu, J. Hou, S. Zheng, W. Xu, Reaction mechanism and influence factors analysis for calcium sulfide generation in the process of phosphogypsum decomposition, Thermochim. Acta 526 (2011) 163-168.

[10] T. Kato, K. Murakami, K. Sugawara, Carbon reduction of gypsum produced from flue gas desulfurization, Chem. Eng. Trans. 29 (2012) 805-810.

[11] Z. Miao, H. Yang, Y. Wu, H. Zhang, X. Zhang, Experimental studies on decomposing properties of desulfurization gypsum in a thermogravimetric analyzer and multi-atmosphere fluidized beds, Ind. Eng. Chem. Res. 51 (2012) 5419-5423.

[12] X. Zhang, X. Song, Z. Sun, P. Li, J. Yu, (2012) Density functional theory study on the mechanism of calcium sulfate reductive decomposition by carbon monoxide, Ind. Eng. Chem. Res. 51 (2012) 6563-6570.

[13] P. Ning, S.C. Zheng, L.P. Ma, Y.L. Du, W. Zhang, X.K. Niu, F.Y. Wang, Kinetics and thermodynamics studies on the decomposition of phosphogypsum in different atmospheres, Adv. Mater. Res. 160-162 (2011) 842-848.

[14] H.F. Mark, D.F. Othtmer, C.G. Overberger, G.T. Seaborg, Kirk-Othmer: Encyclopedia of Chemical Technology, third ed., Wiley-Interscience, New York, 1978.

[15] S. Ruto, J.P. Maree, C.M. Zvinowanda, W.J. Louw, A.V. Kolesnikov, (2011) Thermal studies on gypsum in a pilot-scale rotary kiln, Water in the South African Minerals Industry Conference Proceedings, 15-17 February 2011, The Southern African Institute of Mining and Metallurgy, 2011.

[16] H. Selim, A.K. Gupta, A. Al Shoaibi, Effect of reaction parameters on the quality of captured sulphur in Claus process, Appl. Energy 104 (2013) 772-776.

[17] M.W. Brooks, S. Lynn, Recovery of calcium carbonate and hydrogen sulfide from waste calcium sulphide, Ind. Eng. Chem. Res. 36 (1997) 4236-4242.

[18] M. Garcia-Calzada, G. Marban, A.B. Fuertes, Decomposition of CaS particles at ambient conditions, Chem. Eng. Sci. 55 (2000) 1661-1674.

[19] P. Ballirano, E. Melis, Thermal behaviour and kinetics of dehydration of gypsum in air from in situ real-time laboratory parallel-beam X-ray powder diffraction, Phys. Chem. Minerals 36 (2009) 391-402.

[20] L.S. Clesceri, A.E. Greenberg, R.R. Trussel, Standard Methods for the Examination of Water and Wastewater, seventeeth ed., American Public Health Association, Washington, 1989.

[21] I. Zekker, T. Tenno, A. Selberg, K. Uiga, Dissolution modelling and experimental measurement of CaS-H_2O binary system, Chin. J. Chem. 29 (2011) 2327-2336.

[22] R.C. Weast, CRC Handbook of Chemistry and Physics, fifty-third ed., The Chemical Rubber Co., Cleveland, 1972.

[23] R.H. Perry, Green D., Perry's Chemical Engineers' Handbook, sixth ed. McGraw-Hill Book Company, New York, 1984.

[24] J.A. Dean, Lange's Handbook of Chemistry, fourteenth ed., McGraw-Hill, New York, 1992.

[25] R. Sardeing, J. Aubin, M. Poux, C. Xuereb, Gas-Liquid mass transfer - Influence of sparger location, Chem. Eng. Res. and Des. 82 (2004) 1161-1168.

[26] M. Martin, F.J. Montes, M.A. Galan, Bubbling process in stirred tank reactors II: Agitator effect on the mass transfer rates, Chem. Eng. Sci. 63 (2008) 3223-3234.

[27] S.K. Jana, A.N. Bhaskarwar, Gas absorption accompanied by chemical reaction in a system of three-phase slurry-foam reactors in series, Chem. Eng. Res. and Des. 89 (2011) 793-810.

[28] P.C. Chen, W. Shi, R. Du, V. Chen, Scrubbing of CO_2 greenhouse gases, accompanied by precipitation in a continuous bubble-column scrubber, Ind. Eng. Chem. Res. 47 (2008) 6336-6343.

[29] V.A. Juvekar, M.M. Sharma, Absorption of CO_2 in a suspension of lime, Chem. Eng. Sci. 28 (1977) 825-837.

[30] N. Gehrke, H. Cölfen, N. Pinna, M. Antonietti, N. Nassif, Superstructures of calcium carbonate crystals by oriented attachment, Cryst. Growth Des. 5 (2005) 1317-1319.

[31] A.R. Ibrahim, J.B. Vuningoma, X. Hu, Y. Gong, D. Hua, Y. Hong, H. Wang, J. Li, High-pressure gas-solid carbonation route coupled with a solid ionic liquid for rapid synthesis of rhombohedral calcite, J. Supercrit. Fluids 72 (2012) 78-83.

[32] B. Feng, A.K. Yong, H. An, Effect of various factors on the particle size of calcium carbonate formed in a precipitation process, Mater. Sci. Eng. A 445-446 (2007) 170-179.

[33] I.Robinson, M. Mabuza, S. Mohale, P. Mwape, N. Dlambulo, L. Malebo, M. Ikaneng, R. Motsie, M. Bonga, M. Köhler (Eds), South Africa's Mineral Industry 2011/2012, Department of Mineral Resources, Pretoria, South Africa (2012) pp. 216.

[34] S. Motaung, J. Maree, M. De Beer, L. Bologo, D. Theron, J. Baloyi, Recovery of drinking water and by-products from gold mine effluents, Int. J. Water Res. Dev. 24 (2008) 433-450.

[35] R.E. Vandenberghe, V.G. de Resende, G.M. da Costa, E. De Grave, Study of loss-on-ignition anomalies found in ashes from combustion of iron-rich coal, Fuel 89 (2010) 2405-2410.